



**HAL**  
open science

## Modal and thermal analysis of Les Arches unstable rock column (Vercors massif, French Alps)

Pierre Bottelin, Clara Lévy, Laurent Baillet, Denis Jongmans, Philippe Gueguen

### ► To cite this version:

Pierre Bottelin, Clara Lévy, Laurent Baillet, Denis Jongmans, Philippe Gueguen. Modal and thermal analysis of Les Arches unstable rock column (Vercors massif, French Alps). *Geophysical Journal International*, 2013, 194 (2), pp 849-858. 10.1093/gji/ggt046 . hal-00933213

**HAL Id: hal-00933213**

**<https://hal.science/hal-00933213v1>**

Submitted on 20 Jan 2014

**HAL** is a multi-disciplinary open access archive for the deposit and dissemination of scientific research documents, whether they are published or not. The documents may come from teaching and research institutions in France or abroad, or from public or private research centers.

L'archive ouverte pluridisciplinaire **HAL**, est destinée au dépôt et à la diffusion de documents scientifiques de niveau recherche, publiés ou non, émanant des établissements d'enseignement et de recherche français ou étrangers, des laboratoires publics ou privés.

# Modal and thermal analysis of Les Arches unstable rock column (Vercors massif, French Alps)

P. Bottelin,<sup>1</sup> C. Lévy,<sup>2</sup> L. Baillet,<sup>1</sup> D. Jongmans<sup>1</sup> and P. Guéguen<sup>1</sup>

<sup>1</sup>ISTerre, Université de Grenoble 1, CNRS, IFSTTAR, F-38041 Grenoble, France. E-mail: pierre.bottelin@ujf-grenoble.fr

<sup>2</sup>Géozur, Université de Nice Sophia Antipolis (UNS), CNRS, 250 av Einstein, 06560 Valbonne, France

Accepted 2013 February 4. Received 2012 December 5; in original form 2012 July 4

## SUMMARY

A potentially unstable limestone column ( $\sim 1000 \text{ m}^3$ , Vercors, French Alps) delineated by an open rear fracture was continuously instrumented with two three-component seismic sensors from mid-May 2009 to mid-October 2011. Spectral analysis of seismic noise allowed several resonance frequencies to be determined, ranging from 6 to 21 Hz. The frequency domain decomposition (FDD) technique was applied to the ambient vibrations recorded on the top of the rock column. Three vibration modes were identified at 6, 7.5 and 9 Hz, describing the upper part of corresponding modal shapes. Finite element numerical modelling of the column dynamic response confirmed that the first two modes are bending modes perpendicular and parallel to the fracture, respectively, while the third one corresponds to torsion. Seismic noise monitoring also pointed out that resonance frequencies fluctuate with time, under thermomechanical control. For seasonal cycles, changes in frequency are due to the variations of the bulk elastic properties with temperature. At daily scale, increase in fundamental frequency with temperature has been interpreted as resulting from the rock expansion inducing a closure of the rear fracture rock bridges, hence stiffening the contact between the column and the rock mass. Conversely, the rock contraction induces a fracture opening and a decrease in resonance frequency. In winter, when the temperature drops below  $0^\circ\text{C}$ , a dramatic increase in fundamental frequency is observed from 6 Hz to more than 25 Hz, resulting from ice formation in the fracture. During spring, the resonance frequency gradually diminishes with ice melting to reach the value measured before winter.

**Key words:** Fourier analysis; Geomechanics; Site effects; Early warning.

## 1 INTRODUCTION

In the last two decades, ambient vibrations surveys (Stubbs & McLamore 1973) have been increasingly used for studying the modal properties of civil engineering structures (Sohn *et al.* 1999; Clinton *et al.* 2006; Michel *et al.* 2008; Herak & Herak 2009). Compared to active methods, ambient vibrations are as accurate and offer the advantages of low cost and easy continuous recordings and implementations (Michel *et al.* 2010). Continuous monitoring of dynamic properties (mainly resonance frequencies and damping) can help to detect changes in system stiffness (Doebling *et al.* 1996; Kim & Stubbs 2003). Permanent reduction of resonance frequencies in a Californian building was observed by Clinton *et al.* (2006) after strong earthquake motions, and was interpreted as an indicator of structural damage.

Recently, ambient vibration studies have also been applied on potentially unstable rock slopes. Burjánek *et al.* (2010) and Moore *et al.* (2011) performed seismic noise measurements on the gneissic slope above the Randa scarp (Southern Swiss Alps), which was

generated by two large rockslides in 1991. Polarization analysis revealed a predominant vibration at a given frequency around 5 Hz in the direction of the line of slope, in good agreement with the displacement directions obtained by geodetic measurements. In the same area, processing of the seismic noise registered during 1 hr on the Walkersmaat unstable slope (6 km north of Randa) showed normal mode slope rock vibration around 1.6 Hz, with direction perpendicular to slope surface cracks (Burjánek *et al.* 2012). In the Vercors massif (Western Alps, France), seismic noise was measured during a time period ranging from 6 months to 2 weeks prior to the collapse of a  $21\,000 \text{ m}^3$  limestone column (Lévy *et al.* 2010). Spectral analysis of the signals measured on the column allowed the identification of several resonance frequencies, which were not observed on the rock massif records. The lowest resonance frequency showed a significant drop (from 3.4 to 2.6 Hz) 2 weeks before the fall, which was interpreted as the breakage of rock bridges, also attested by the increase in seismic activity. These results illustrate that the damaging process on both natural and man-made structures can be tracked by changes in resonance frequency.

However, monitoring studies on buildings and unstable slopes both revealed that the resonance frequencies also exhibit significant reversible variations. Indeed, weather conditions such as air temperature and humidity have a substantial effect on the resonance frequencies of civil engineering structures (Clinton *et al.* 2006; Yuean & Kuok 2010; Mikael *et al.* 2012) and rock column (Lévy *et al.* 2010). For a reinforced concrete slab exposed to a 20 °C temperature fluctuation, Xia *et al.* (2010) observed 3 per cent variation in fundamental frequency. In buildings, Nayeri *et al.* (2008) reported 1 per cent wanders in fundamental frequency under natural temperature fluctuations. In their study on the prone-to-fall rock column, Lévy *et al.* (2010) found that a temperature variation of 20 °C generated a reversible change of about 5 per cent in the first resonance frequency. Therefore, frequency fluctuations induced by thermal effects can mask small structural changes caused by damaging, both in civil engineering and rock mechanics. Discriminating reversible temperature effects from irreversible damaging effects is then required for resonance frequency monitoring. Although several techniques have been proposed for civil engineering structures such as reinforced concrete beams or buildings (Yuean & Kuok 2010; Lin *et al.* 2011), there is currently no easy and validated method to tackle this problem.

This study aims at focusing on the factors influencing the dynamic response of a prone-to-fall rock column, located hundred metres to the south of that studied by Lévy *et al.* (2010). The top of this column was equipped with two three-component (3-C) seismometers during 29 months. First, the spectral analysis of ambient vibrations evidenced the existence of several resonance frequencies varying with time. Then, the application of the frequency domain decomposition (FDD) method (Brincker *et al.* 2001) and 3-D numerical modelling allowed identifying the modes corresponding to the first three resonance frequencies. Finally, the temperature control on the fundamental mode was experimentally and numerically studied.

## 2 FIELD SITE

The study site is located to the South of the carbonate Vercors Massif (western Alps, France), at about 1900 m in elevation (Fig. 1a). This part of the Vercors Massif is a plateau limited by an east-facing cliff made of near-horizontal metre-thick bedded limestone in its upper part (highest 100 m), while marly limestone composes the less steep lower part of the cliff with few decimetres thick layers.

The rock column was identified as potentially unstable in 2007 November, after the collapse of a similar and nearby larger column (Lévy *et al.* 2010). A Lidar scan of the cliff was acquired in 2007 December, using a Riegl 2-D laser scan put together with a Hasselblad digital camera, an Inertial Measurement Unit iMAR and a Dual frequency GNSS receiver. The Digital Elevation Model (D.E.M.) derived from Lidar data is shown in Fig. 1(b). The column, which is 30 m high, about 15 m wide and 5 m thick at its top, is separated from the massif by a 0.7 m wide open rear fracture extending to a depth estimated at about 15 m. This last value is however little constrained. The total unstable volume was estimated at about 1000 m<sup>3</sup>. Water seepage was observed at the toe of the column, where ice develops during winter.

In 2009 May, the site was equipped with two 2 Hz seismometers: one vertical on the stable massif and one 3-C on the unstable rock column. The seismic station was configured to record microcracks (Lévy *et al.* 2011) and operated in a triggered mode using an *STA/LTA* criterion (*STA* = 0.5 s, *LTA* = 20 s, *STA/LTA* > 6) with 1000 Hz of sampling frequency from 2009 May until 2010 June. Time windows of at least 2 min were recorded, allowing seismic noise signals to be extracted. The array configuration changed to three 2 Hz 3-C seismometers after 2010 June (labelled S1 to S3, Fig. 1c) and seismic recordings were continuously acquired using a

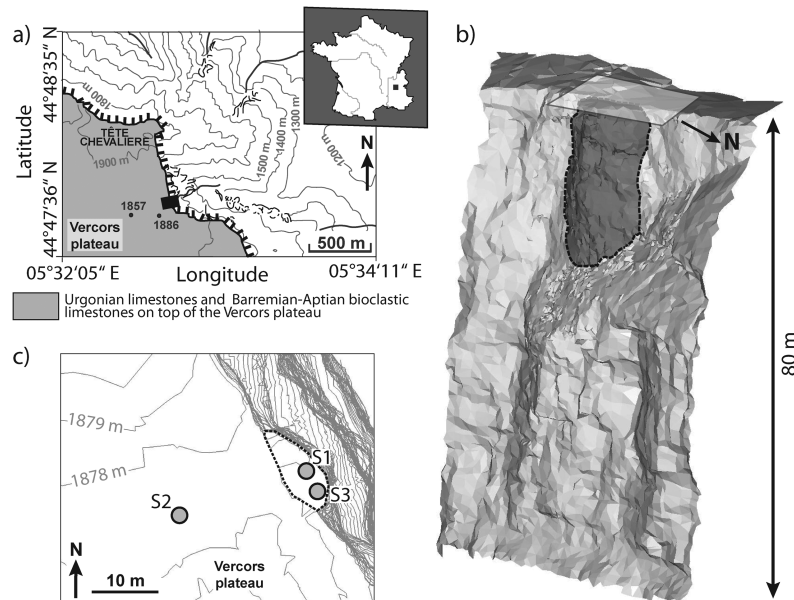


**Figure 1.** (a) Situation map of the study site located at the border of the Vercors plateau (southeast of France). The cliff limit is delineated with a barbed line and the site is located with a black rectangle. Grey area corresponds to Barremian bioclastic limestone. (b) Digital elevation model of the cliff obtained from Lidar data. The location of the sensor array is indicated by a white transparent parallelogram. The extension of the rock column, deduced from morphology and fracture analysis, is outlined with a dark dashed line. Water seepage is observed at the toe of the column. (c) Top view of the equipment layout at the experimental site. From 2009 May to 2010 June, the seismic array was composed of one vertical seismometer S2 (2 Hz) on the stable massif and one 3-C seismometer S1 on the unstable rock column. Afterwards, the array configuration changed to three 3-C seismometers (S1, S2 and S3). The limits of the unstable column are delineated by a black dashed line.

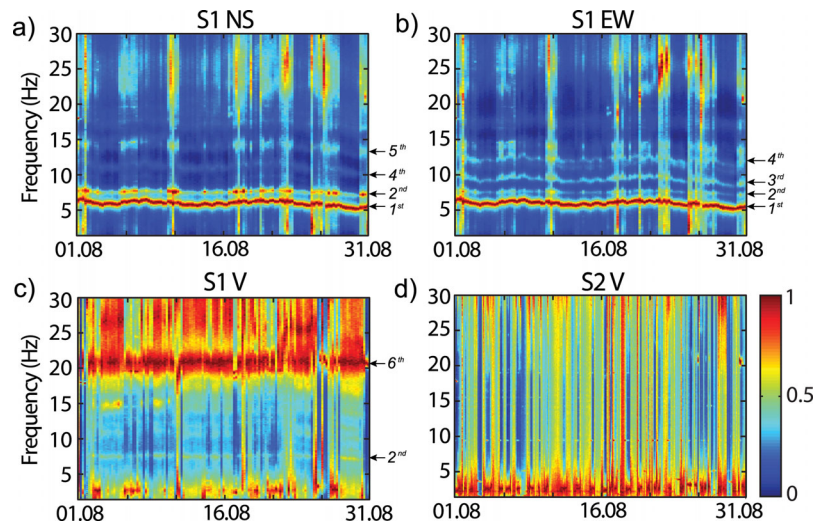


**Figure 2.** Normalized Fourier spectra of seismic noise recorded during 2009 August by the 3C sensor installed on the unstable rock column (a) NS horizontal component, (b) EW horizontal component and (c) vertical component. (d) Same plot for the vertical sensor S2 installed on the stable massif. The frequency peaks are pointed by the black arrows on the right-hand side and referenced in Table 1.

250 Hz sampling frequency. Air temperature under shelter, rainfall and wind speed were recorded every 15 min by the permanent meteorological station ‘Jardins du Roi’, located 3.2 km southwest of the site and 120 m below in altitude. Both seismic and meteorological data are time-referenced in UTC.

### 3 SEISMIC NOISE CHARACTERISTICS

Spectral characteristics of the seismic noise recorded on the column and on the stable massif were first studied over a short period of time (2009 August). Fourier spectra were computed from the triggered recordings, using 5 s windows selected with an antitriggering filter ( $STA/LTA < 2$ ,  $STA = 0.5$  s,  $LTA = 20$  s). These spectra were then stacked to reach the equivalent of 1 hr of noise record (i.e. 720 5 s time segments). For a better legibility, each spectra stack was normalized to one over the whole frequency range. Figs 2(a)–(c) present normalized stacks of seismic noise spectra (further referred as ‘spectra’) during 2009 August for the 3C sensor S1 installed on the unstable column. The two horizontal components (North–South in Fig. 2a and East–West in Fig. 2b) show a frequency peak around 6 Hz, which slightly fluctuates with time. Other frequency peaks at about 7.5, 9 and 11 Hz are observed on one or the two horizontal components (see arrows in Figs 2a–c). Although they are less energetic than the first peak, they exhibit similar fluctuation patterns. Only two frequency peaks (at 7.5 and 21 Hz) were spotted on the vertical component spectra (Fig. 2c), the dominant peak at 21 Hz not being perceptible on the horizontal components.

In contrast, the vertical sensor S2 located on the stable massif shows no distinct peak in the same frequency range (Fig. 2d). The spectra are characterized by high amplitudes at low frequencies (<3 Hz). This difference in frequency response between sensors S1 and S2 reveals the resonance of the unstable column. The frequency peaks appearing on the unstable rock column are listed in Table 1, and show some purely horizontal modes (6, 9 and 11 Hz), one vertical mode (21 Hz) and a compound mode (7.5 Hz). Further study of the column resonance modes will be carried out in Section 4.

**Table 1.** Frequency peaks for the 3C seismometer S1 installed on the unstable rock column.

Frequency peak	Component		
	S1 V	S1 NS	S1 EW
First		6 Hz	6 Hz
Second	7.5 Hz	7.5 Hz	7.5 Hz
Third		11 Hz	11 Hz
Fourth		15 Hz	
Fifth			
Sixth	21 Hz		

## 4 MODAL ANALYSIS OF THE UNSTABLE ROCK COLUMN

### 4.1 Application of the FDD method

The FDD method uses a decomposition of the spectral density function matrix to separate the response spectra into a set of single degree of freedom systems, each corresponding to an individual mode (Brincker *et al.* 2001). It was applied to ambient vibrations measured by the two 3C seismometers S1 and S3 located on top of the rock column, to identify the modal shapes corresponding to the observed resonance frequencies. 1-hr-long recordings dating back from the 2011 November 30 were selected for the analysis. Three frequency peaks fitting a Modal Assurance Criterion (Allemang & Brown 1982) above 80 per cent over large frequency bands (>1 Hz) were identified ( $f_1 = 5.95$  Hz,  $f_2 = 6.94$  Hz and  $f_3 = 8.80$  Hz, Fig. 3a and Table 2). Although higher modes probably exist (see Fig. 2), they were not evidenced by the FDD method because of lower modal participation factors and weak amplitude of the excitation at high frequency. The identified modes were interpreted as the three first resonance modes of the column. The measured frequencies are comparable with the first three frequency values given in Table 1, but are slightly lower probably because of the difference in time between the recordings (2011 November versus 2009 August). These results highlight some fluctuations of these frequencies with time, which will be studied in Section 5.

Due to topographical reasons, ground vibration was recorded only at two points on the top of the rock column, allowing reconstructing the upper motion of each modal shape. Fig. 3(b) shows

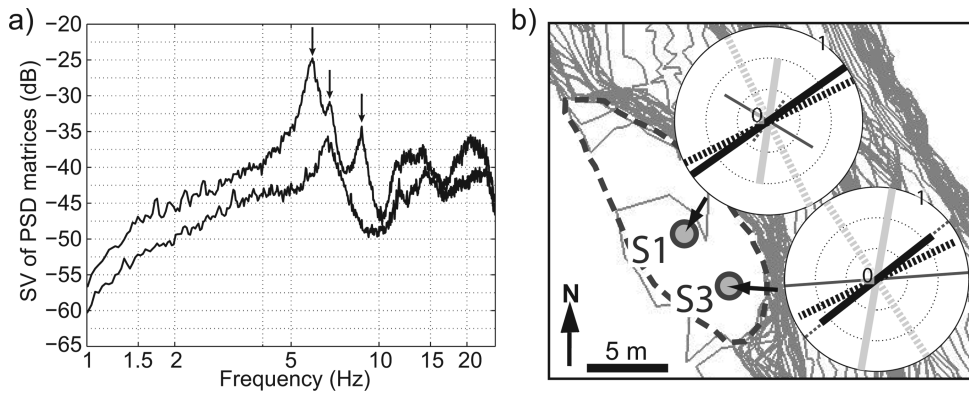


**Figure 3.** (a) Plot of the first (top) and second (bottom) singular values (SV) of power spectrum density (PSD) matrices computed by the frequency domain decomposition method. Three resonance frequencies showing a high modal assurance criterion ( $> 80$  per cent) over large frequency bands ( $> 1$  Hz) are identified at  $f_1 = 5.95$  Hz,  $f_2 = 6.94$  Hz and  $f_3 = 8.80$  Hz (black arrows). (b) Top view of the horizontal motions for the first three resonance modes at sensors S1 and S3. Motions determined by FDD and numerical modelling are shown with solid and dashed lines, respectively. The three first resonance modes are outlined by thick black ( $f_1$ ), thick light grey ( $f_2$ ) and thin dark grey ( $f_3$ ) lines. For each mode, the amplitude of motion is normalized to 1.

**Table 2.** Comparison of resonance frequency for the three first modes calculated using the FDD method and 3-D numerical modelling.

Method	$f_1$ (Hz)	$f_2$ (Hz)	$f_3$ (Hz)
FDD	5.95	6.94	8.80
Numerical modelling	4.06	8.06	10.84

the normalized motions for the three first resonance modes in thick black, thick light grey and thin dark grey solid lines, respectively. All three motions are mainly horizontal, which explains why they were hardly distinguished on the vertical component of the sensor installed on the column (S1 V, Fig. 2c). Horizontal motions of the two first modes are parallel and in phase at the two sensors, corresponding probably to bending modes parallel and perpendicular to the rear fracture, respectively. In contrast, the third mode exhibits non-parallel motions, which suggest torsion around the vertical axis. These inferences will be compared in the next section with 3-D numerical modelling simulations.

#### 4.2 3-D numerical modal analysis of the unstable rock column

To validate this interpretation, 3-D numerical modelling of the rock column response was performed using the continuous-medium finite-element software *Comsol* (<http://www.comsol.com>). Computations were made using automatic meshing with tetrahedral finite elements. The D.E.M. shown in Fig. 1(b) was used for defining the column geometry and an open 15-m-deep rear fracture was considered. Mechanical embedding was applied on the rock massif boundaries. The mechanical properties of the material were derived from a previous seismic study conducted in the same area (see Lévy *et al.* 2010). Assuming the material is isotropic and homogeneous with a density of  $2650 \text{ kg m}^{-3}$ , and neglecting the superficial thin layer of soil, a Young's modulus  $E = 6.9 \cdot 10^9 \text{ Pa}$  and a Poisson ratio  $\nu = 0.43$  were computed. These values characterize the fractured rock mass at the scale of the seismic wavelength (20–40 m).

Numerical modelling with these parameters gives resonance frequency values of 4.06, 8.06 and 10.84 Hz for the three first modes. Although these values are in the range of the measured frequencies (see comparison in Table 2), the lowest and highest computed resonance frequencies are underestimated and overestimated, respec-

tively. Considering the uncertainty on the input parameters (e.g. the geometry of the open rear fracture), numerical simulations will thus help to semi-quantitatively interpret the observations. The 3-D column displacement fields (Fig. 4) show that these three modes correspond to lateral bending, transverse bending and torsion, respectively. In particular, the first resonance frequency, measured around 6 Hz with ambient vibrations, corresponds to the first flexion mode of the rock column in the direction perpendicular to the rear fracture. Horizontal motions for these three first modes at sensors S1 and S3 (dashed lines) are compared to the results of the FDD method in Fig. 3(b). The agreement between motion directions is very good for the first mode, while the second and third modes exhibit significant differences in motion directions ( $30\text{--}45^\circ$ ). The main uncertainty on the input parameters is the extent of the rear fracture, which strongly controls the column dynamic response. Additional numerical simulations were computed with different rear fracture depths. Results (not shown here) confirmed the nature of the three first modes, with two bending and one torsion modes. The first one is always a bending mode vibrating in the direction perpendicular to the rear fracture, whose frequency changes with the fracture depth. On the contrary, the direction of vibration of the two higher modes turned out to be more sensitive to the fracture geometry, explaining the discrepancy between observations and modelling.

#### 5 THERMAL INFLUENCE ON THE COLUMN RESONANCE

The normalized Fourier spectra of seismic noise (recorded on the horizontal East–West component of sensor S1 located on the column) are displayed in Fig. 5(a) between 2009 May and 2011 October. The first resonance frequency  $f_1$  is clearly visible (black arrow) and exhibits significant fluctuations from 5 Hz in autumn to more than 25 Hz in winter. Two other modes, less energetic, are visible between 7 and 15 Hz. Air temperature and daily rainfall recorded at the weather station are shown in Fig. 5(b). During positive temperature periods (from May to October),  $f_1$  decreases from 7.5 Hz to about 5 Hz. In contrast, when the temperature drops below  $0^\circ \text{C}$ , (November to April),  $f_1$  sharply increases and remains high during the freezing periods, peaking at about 25 Hz in 2010 January and 2011. Fourier spectra of the temperature and  $f_1$  curves (not shown) evidence predominant peaks at 1 day and 1 year period. The two curves were both bandpass filtered at 1 year (Fig. 6a) and

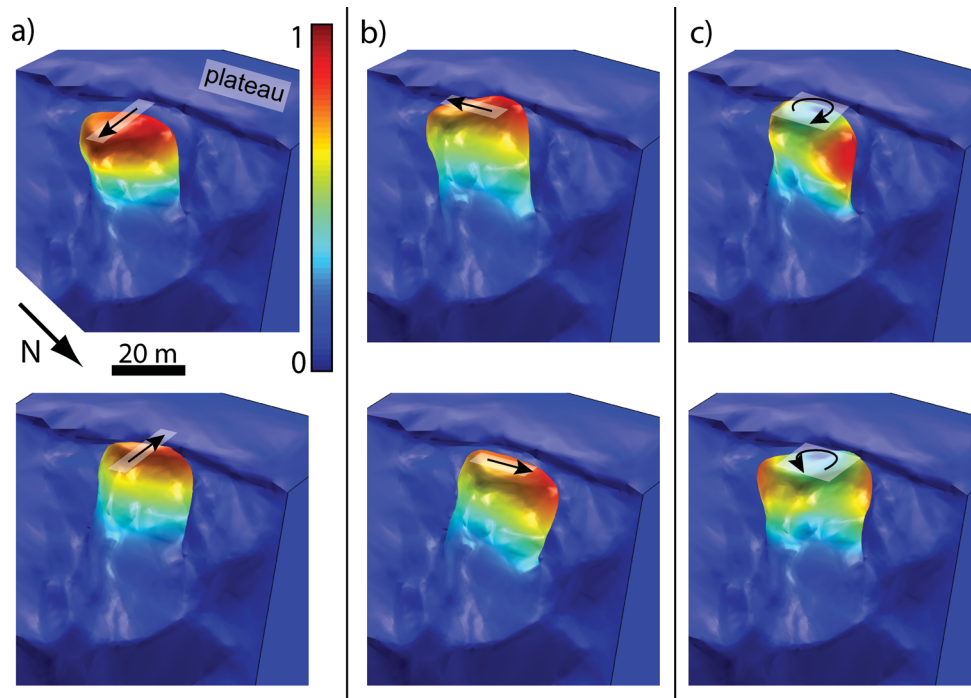


**Figure 4.** 3-D maximum amplitude displacements of the column for the three first resonance modes (15 m deep rear fracture). Motion scale is normalized by the maximal displacement for each mode. (a) bending mode perpendicular to the cliff at 4.06 Hz, (b) bending mode parallel to the cliff at 8.06 Hz and (c) torsion mode at 10.84 Hz (c).

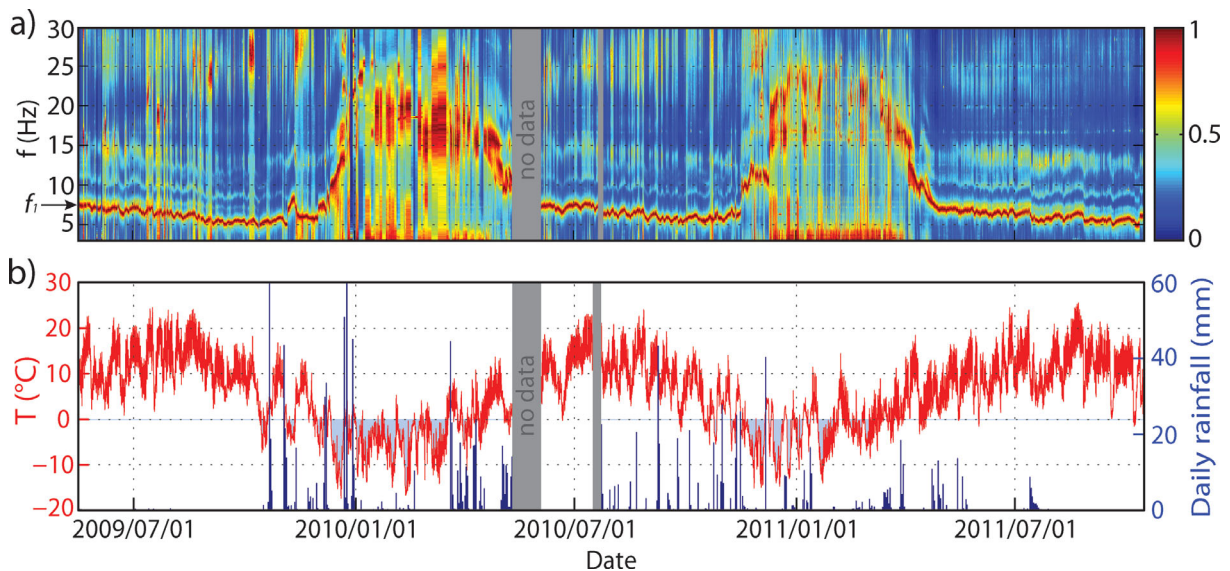


**Figure 5.** (a) Normalized Fourier spectra of seismic noise recorded by the EW horizontal component of S1 installed on the unstable rock column, from 2009 May to 2011 October. The first resonance frequency ( $f_1$ ) is shown by the black arrow. (b) Climatic parameters recorded over the same time span. Air temperature under shelter and daily rainfall are shown by the red line and the blue bars, respectively. Freezing periods are outlined in light blue.

1 day (Fig. 6b) periods and the corresponding intercorrelations are displayed in Figs 6(c)–(e), respectively. In the following, the study of the relation between temperature and  $f_1$  is consequently split into three parts: freezing periods, yearly changes and daily variations.

### 5.1 Freezing periods

At the beginning of the freezing periods (outlined by light blue areas in Fig. 5b),  $f_1$  dramatically increases to reach 25 Hz at maximum.

to understand this phenomenon, we studied the first freezing events of the 2010–2011 winter (occurring from October to December; Fig. 7). The first negative temperature occurrence (G1 event) did not provoke a significant increase in resonance frequency. In contrast, a dramatic  $f_1$  augmentation occurred during the G2 and G3 events that however exhibit a similar temperature drop. The main difference between G1 and these two episodes is that the latter were preceded by heavy rainfall. The same observation can be made for the sharp increase in  $f_1$  (over 10 Hz) resulting from the severe temperature drop during event G4. These results suggest that the

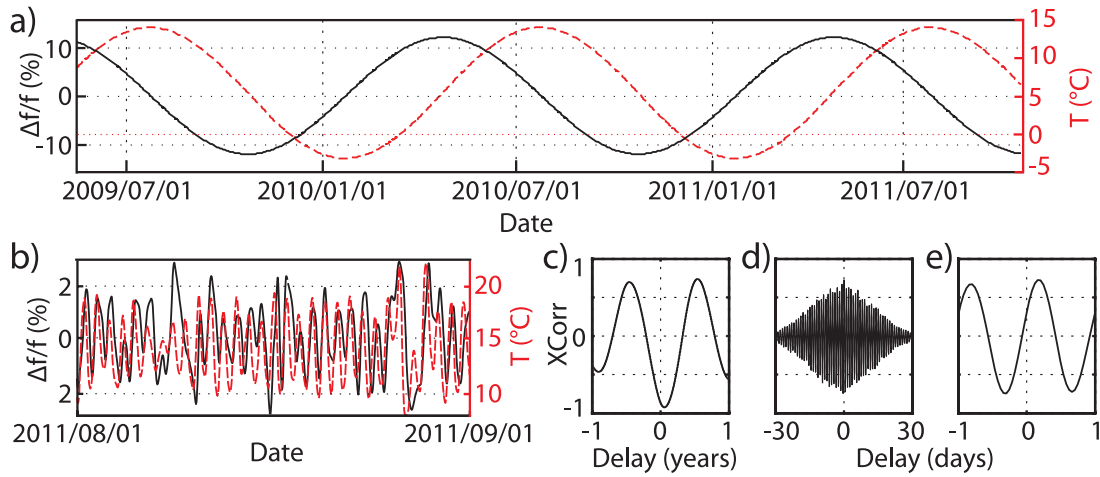


**Figure 6.** (a) First resonance frequency (yearly bandpass-filtered, zero-centred and normalized, in continuous black line) and air temperature variations (yearly bandpass-filtered, in red dashed line) displayed over two and a half years. (b) Daily bandpass-filtered variations of temperature and frequency during 2011 August. (c) Cross-correlation between yearly variations of temperature and frequency (Fig. 5a). (d) Cross-correlation between daily variations of temperature and frequency (Fig. 5b). (e) Zoom of Fig. 5(d) in the  $(-1 \text{ } 1 \text{ day})$  delay range.

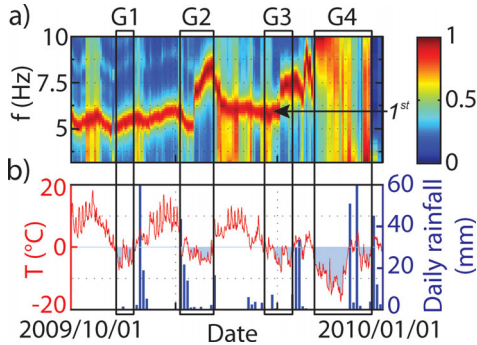


**Figure 7.** (a) Normalized Fourier spectra of seismic noise recorded on the EW horizontal component (S1) installed on the unstable rock column from 2009 October to 2011 January. The first resonance frequency is pointed by a black arrow. (b) Air temperature (red line) and rainfall (blue bars) measured at the weather station 'Jardins du Roi', 3.2 km to the southeast from the field site. Freezing periods G1, G2, G3 and G4 are filled with light blue and outlined by black rectangles.

increase in  $f_1$ —which typically spans over 1 or 2 days—is related to the transformation of water into ice. Ice formation in rock cracks raises the bulk stiffness of the rock material (Bost 2009), increasing the column resonance frequency. Ice also probably developed in the main rear fracture, stiffening the contact between the column and the rock mass. This hypothesis is supported by the observation of water seepage at the bottom of the column in autumn that turns into ice accumulation in winter. Data then suggest that water availability and freezing intensity control ice formation (Matsuoka 2001), which plays a major role in the increase of  $f_1$ .

## 5.2 Yearly variations

During non-freezing periods (May–October), the first resonance frequency  $f_1$  and temperature curves oscillate around a mean value, following seasonal cycles (Fig. 5). Sinusoid curves were fitted in the least-squares sense, excluding the freezing periods for  $f_1$ . Fig. 6(a) presents the harmonic variations of  $f_1$  (zero-centred and normalized) and of the temperature over time.  $f_1$  oscillates around 6.28 Hz with an amplitude of  $\pm 0.78 \text{ Hz}$  (12 per cent variation) while temperature

varies in the range  $\pm 8.7 \text{ }^\circ\text{C}$  over time, around a mean  $5.4 \text{ }^\circ\text{C}$  value. Cross-correlating these two curves (Fig. 6c) yields a high correlation coefficient of  $-0.92$  (opposition in phase) with a delay of 87 days.

A simple computation was carried out using 1-D heat conduction equations (Lowrie 2007) to understand this delay:

$$\Delta T(z, t) = \Delta T_0 \cdot e^{-\frac{z}{d}} \cdot \cos\left(\omega t - \frac{z}{d}\right) \quad (1)$$

with

$$d = \sqrt{\frac{2D}{\omega}}, \quad (2)$$

where  $z$  is the distance between the surface and the point considered into the rock mass (in meters),  $t$  is the time (in seconds),  $\omega$  is the angular frequency of temperature variation at surface (in  $\text{rad s}^{-1}$ ),  $T$  is the temperature (in  $^\circ\text{C}$ ),  $T_0$  is the temperature at surface (in  $^\circ\text{C}$ ) and  $D$  is the thermal diffusivity (in  $\text{m}^2 \text{ s}^{-1}$ ) given by:

$$D = \frac{\lambda}{\rho c_p}. \quad (3)$$

The following usual characteristics were retained for the rock material (after Lowrie 2007): thermal conductivity  $\lambda = 1 \text{ W m}^{-1} \text{ }^\circ\text{C}^{-1}$ , heat capacity at constant pressure  $C_p = 800 \text{ J kg}^{-1} \text{ }^\circ\text{C}^{-1}$ , density  $\rho = 2650 \text{ kg m}^{-3}$  (Table 3). Calculations show that after 87 days (delay observed between air temperature and  $f_1$  changes), the heat wave front is located at 3.3 m in depth. As the 4-m-thick rock column is surrounded by air, its whole volume is probably affected by a temperature change at this time. Therefore, the delay observed

**Table 3.** Mechanical and thermal parameters used for simulation.

Parameter (units)	Value
Density $\rho$ ( $\text{kg m}^{-3}$ )	2650
Young's modulus $E$ (MPa)	6900 <sup>a</sup>
Poisson ratio $\nu$	0.43
Thermal conductivity $\lambda$ ( $\text{W m}^{-1} \text{ K}^{-1}$ )	1
Coefficient of thermal expansion $\alpha$ ( $^\circ\text{C}^{-1}$ )	$3 \cdot 10^{-6}$
Heat capacity at constant pressure $C_p$ ( $\text{J kg}^{-1} \text{ }^\circ\text{C}^{-1}$ )	800
Heat transfer coefficient $h$ ( $\text{W m}^{-2} \text{ }^\circ\text{C}^{-1}$ )	1–20

<sup>a</sup>Here given at  $T = 20 \text{ }^\circ\text{C}$ .

between the temperature and frequency fluctuations suggest that the physical process controlling the resonance frequency at yearly scale takes place into the rock volume. That could result from the dependence of the bulk rigidity behaviour on temperature, and this hypothesis will be discussed in Section 7.

### 5.3 Daily variations

Fig. 6(b) shows the daily-filtered variations of fundamental frequency (zero-centred and normalized) and temperature in 2011 August. During this non-freezing period, the two curves exhibit oscillations between  $\pm 3^\circ\text{C}$  and  $\pm 0.1$  Hz, respectively, with a short delay between a temperature change and the corresponding frequency response. Cross-correlating the two curves (Figs 6d and e) gives a maximal 0.7 coefficient of correlation, with a 4.5 hr delay of  $f_1$  with respect to temperature.

Preliminary one-dimension conduction study using the same parameters as in Section 5.2 showed that the perturbation in temperature into the rock mass is negligible (i.e. <1 per cent of the air temperature change) at depth greater than 0.57 m. The heat wave front penetration corresponding to a 4.5 hr delay is only 0.13 m, meaning that only the superficial skin of the 4-m-thick rock column is affected by a temperature change. This result suggests that the physical processes controlling the evolution of the first resonance frequency at daily timescale occur in the superficial area of the rock column.

In summary, the study of the temperature influence on the first resonance frequency  $f_1$  has evidenced an opposite effect: at the day scale, the two curves are in phase with a small delay of a few hours, while at the year scale the two parameters are anticorrelated with a delay of about 3 months. In the next section, an attempt is made to understand these relations, using thermomechanical modelling.

## 6 THERMOMECHANICAL NUMERICAL MODELLING

The thermomechanical behaviour of the rock column was modelled using *Comsol* software. The 2-D geometry of the column derived from the D.E.M. is shown in Fig. 8(a), as well as the boundary conditions. The bottom and left sides (A and B) of the model are thermally insulated and mechanically embedded, while all other surfaces (C–E) are free to move.

The relation between the air temperature and the rock surface temperature is driven by the convection phenomenon, obeying the following law (Jiji 2010):

$$\mathbf{n} \cdot (\lambda \nabla T) = h(T_a - T_s), \quad (4)$$

where  $\mathbf{n}$  is the unit vector normal to the surface,  $\lambda$  is the thermal conductivity ( $\text{W m}^{-1} \text{C}^{-1}$ ),  $T_a$  and  $T_s$  are the air and rock surface temperatures, respectively, and  $h$  is the heat transfer coefficient ( $\text{W m}^{-2} \text{C}^{-1}$ ).

For both the ground surface and the eastward cliff face, facing free-air, the heat transfer coefficient ( $h$ ) is chosen equal to

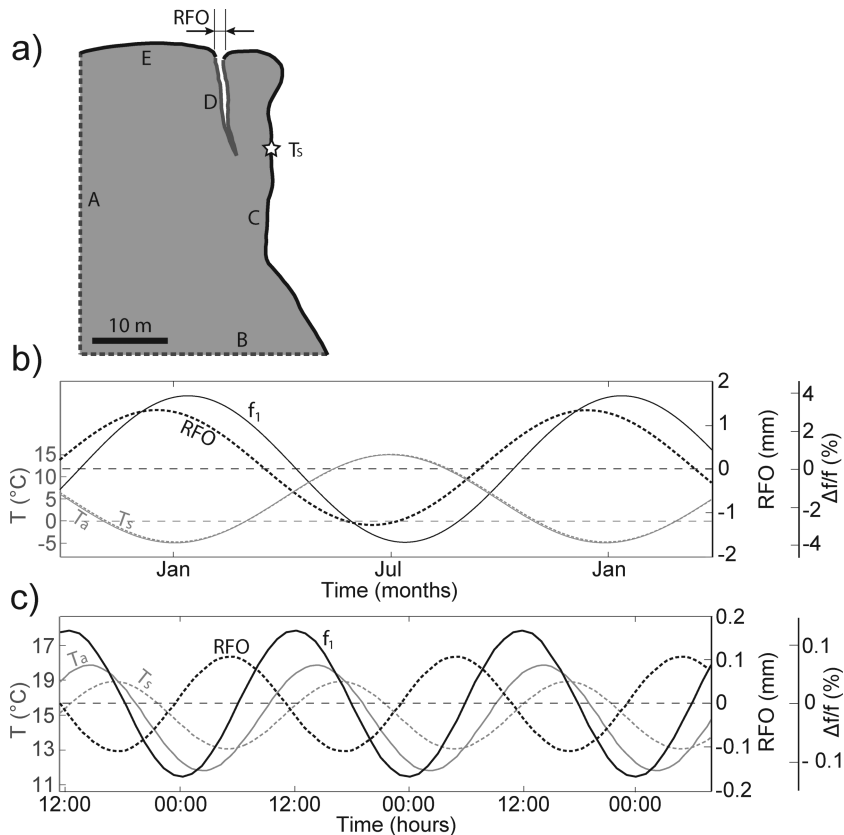


**Figure 8.** Thermal modelling of the column. (a) 2-D section of the model and boundary conditions. No heat flux is applied along boundaries A and B (grey dashed line), while faces shown by black (C and E) and grey (D) plain lines are affected by convection with a heat transfer coefficient of 20 and  $1 \text{ W m}^{-2} \text{C}^{-1}$ , respectively. The point where the surface temperature ( $T_s$ ) is measured is located by a white star. (b) Modelled yearly variations of  $f_1$  (first resonance frequency) and RFO (rear fracture opening) are shown in plain and dashed black lines, respectively, along with the air ( $T_a$ ) and rock surface ( $T_s$ ) temperatures (plain and dashed grey lines, respectively). (c) Same as (b) for daily variations. Zero line is outlined by grey dashed horizontal lines.

$20 \text{ W m}^{-2} \text{ } ^\circ\text{C}^{-1}$  (Bergman *et al.* 2011), while  $h$  is lowered to  $1 \text{ W m}^{-2} \text{ } ^\circ\text{C}^{-1}$  in the rear fracture, accounting for a less efficient convection process.

Heat transfer into the rock material is assumed to occur only by conduction in this first approach. This hypothesis may not be fully satisfied, owing to the presence of discontinuities and pores in the material (Gruber & Haerberli 2007). All the mechanical and thermal parameters used in this section are given in Table 3.

Assuming constant Poisson's ratio and density, the thermomechanical coupling was introduced using the following linear relationship (Xia *et al.* 2010), between the Young's Modulus  $E$  and the temperature  $T$ :

$$E(T) = E(T_{\text{ref}})[1 - \theta(T - T_{\text{ref}})], \quad (5)$$

where  $E$  is the Young's modulus,  $T$  is the temperature of the material,  $T_{\text{ref}}$  is a reference temperature (chosen equal to  $20 \text{ } ^\circ\text{C}$ ) and  $\theta$  is the temperature coefficient of Young modulus, depending on the material. This equation was initially proposed for concrete with  $\theta = 0.003$  (Xia *et al.* 2010). Using  $P$ -wave velocity values measured in limestone enduring freeze/thaw cycles in the range  $\pm 20 \text{ } ^\circ\text{C}$  (Tourenq 1970) and assuming a constant value for the Poisson coefficient, the coefficient  $\theta$  was determined to be 0.012 and 0.03 for dry and saturated rock, respectively. Daily and yearly variations of the rear fracture opening (RFO) and the first resonance frequency ( $f_1$ ) were computed for dry rock conditions, hypothesis which will be discussed later.

### 6.1 Yearly variations

The rock surface temperature,  $f_1$  and RFO curves were computed during 18 months for air temperature fluctuations of  $\pm 10 \text{ } ^\circ\text{C}$  around a mean value of  $5 \text{ } ^\circ\text{C}$  (Fig. 8b). At this timescale, the air and rock surface temperature curves are almost superimposed, while the RFO, which oscillates in the range  $\pm 1.4 \text{ mm}$ , is anticorrelated with temperature. Surprisingly, the RFO maximum is reached a few days before the rock surface temperature peak. Relative variations in  $f_1$  ( $\pm 4$  per cent, Fig. 8b) are clearly anticorrelated with air temperature, with a correlation coefficient of  $-0.99$  and a 14 day delay. These numerical results are globally consistent with field measurements, although differences appear in the frequency variations and delay values. At the year scale, the whole column volume is affected by the temperature variations. A rise in temperature provokes a diminution of the Young's modulus and a decrease in  $f_1$ , explaining the anticorrelation observed between air temperature and  $f_1$ . The computed relative frequency variations ( $\pm 4$  per cent) are lower than those measured ( $\pm 12$  per cent), and are mainly controlled by coefficient  $\theta$  (eq. 5). Dry rock conditions ( $\theta = 0.012$ ) were chosen for simulation, because of the presence of open fractures draining the column. However, water seepage observed at the column base suggests that a part of the column could be wet, rising  $\theta$ . The same computations made for saturated conditions ( $\theta = 0.03$ ) yield relative frequency variations of  $\pm 21$  per cent, which overestimate the observations. Simulation results for extreme hydrogeological conditions (dry and saturated rock) are then bracketing the observed frequency variations. A significant discrepancy was found between the observed and simulated delays (87 and 14 days, respectively). It could result from inadequate input parameter values (too high thermal conductivity, for instance), which were not measured for this specific rock. Also, the one order of magnitude drop in rock thermal diffusivity resulting from the freezing of the liquid water fraction (Wegmann *et al.* 1998; Kukkonen & Safanda 2001; Gruber & Haerberli 2007;

Noetzli *et al.* 2007) was not considered in this study and could have delayed the thermal wave front propagation.

The opening of the rear fracture with the temperature decrease was interpreted as resulting from the rock thermal contraction. A detailed analysis of the numerical results showed that the observed RFO advance on air temperature (Fig. 8c) results from complex thermal conduction process in 2-D geometry.

Presence of ice into the rear fracture stiffens the massif/column interface in the winter months, leading to a dramatic increase in first resonance frequency from 6 to about 25 Hz (see Section 5). 2-D numerical modelling of the column with a 15 m high rear fracture (Fig. 8a) was performed, introducing different ice heights in the fracture. As the Young's modulus of ice at  $-10 \text{ } ^\circ\text{C}$  (about 10 GPa; Petrovic 2003) is close to the rock modulus measured at Les Arches in summer (6.9 GPa), the same mechanical characteristics were considered for both materials. It turned out that about 7 m thickness of filling ice (about half the fracture height) is required to explain the observed 300 per cent  $f_1$  augmentation.

### 6.2 Daily variations

Daily variations of the same parameters were simulated in summer conditions during 3 days for air temperature oscillating with  $\pm 3 \text{ } ^\circ\text{C}$  in amplitude around a mean value of  $14.2 \text{ } ^\circ\text{C}$  (Fig. 8c). Temperature of the rock surface follows the air temperature variation with a 2.75 hr delay and a reduction of 40 per cent in amplitude resulting from the thermal convection process. The RFO, which varies in the range  $\pm 0.1 \text{ mm}$ , is almost in opposition of phase with the rock surface temperature change (slight half-hour delay). Numerical tests showed that these opening fluctuations result from the thermal contraction and expansion affecting the east-facing cliff and, to a less extent, the fracture walls. The relative variation in  $f_1$  (Fig. 8c), which results from the change in Young's modulus with temperature, is weaker (0.13 per cent) than that observed (2 per cent in Fig. 6b) and the modelled curve  $f_1$  is in opposition of phase with the air temperature, contrary to the experimental curve. Indeed, at the daily scale, the heat wave front penetrates only a few tens of centimetres deep into the rock mass with a delay of about a few hours, and then little affects the resonance frequency. On the contrary, in open fractures, daily temperature variations could change the contact near rock bridges, which were shown to play a major role on the first resonance frequency (Lévy *et al.* 2010). Our interpretation is that the temperature increase in the open rear fracture induces local rock thermal expansion that closes microcracks near rock bridges and increases the contact surface. That stiffens the contact between the column and the rock mass and raises the first resonance frequency. A decrease in temperature generates the opposite effect.

## 7 CONCLUSIONS

The combined analysis of field measurements and numerical modelling has given insight into the thermomechanical behaviour of the Les Arches unstable rock column and has evidenced a different response under daily and yearly temperature cycles.

Seismic noise measurements during two and a half years have shown that the column vibrates predominantly at its first resonance frequency  $f_1$ , which exhibits daily and yearly fluctuations.  $f_1$  variations show distinct characteristics according to the periodicity, and are probably due to thermal control of the column dynamic response. Thermomechanical numerical modelling was hence used to understand the column behaviour.

At the year scale, the  $f_1$  curve exhibits a dissymmetric shape with a sharp increase (from about 5 to more than 25 Hz) during freezing periods preceded by rainfalls (Fig. 5). These observations, along with numerical modelling, suggest that this dramatic augmentation in resonance frequency is linked to ice growth in the rear fracture, stiffening the contact between the rock mass and the column. Once the ice has melted, the  $f_1$  curve exhibits a yearly harmonic variation controlled by seasonal temperature fluctuations which alter the Young's modulus of the rock. A temperature maximum (minimum) is followed by a  $f_1$  minimum (maximum) with a delay of about 3 months.

At the daily scale, the  $f_1$  and air temperature curves are in phase, with a delay of a few hours. The thermomechanical modelling of the column, assuming a lowering of the mechanical modulus with temperature, yielded a decrease in  $f_1$  with temperature with a relative variation of one order of magnitude lower ( $10^{-2}$  Hz) than that observed ( $10^{-1}$  Hz). Therefore, an increase in  $f_1$  probably results from the stiffening of the interface between the column and the rock mass due to thermal expansion, and reciprocally.

The significant reversible thermal effects evidenced in this study could mask the irreversible decay in  $f_1$  resulting from rock damaging. In the future, discriminating methods have to be developed for enabling to use the reduction in  $f_1$  as a precursor for rock falls.

## ACKNOWLEDGEMENTS

This work was partially funded by the federative structure V.O.R. (Vulnérabilité des Ouvrages aux Risques) and the Alcotra project MASSA. This work would not have been achieved without the help of many field work participants; we are especially grateful to L. Darras, J. Turpin, G. Cougoulat and R. Béthoux. Thanks to the Vercors Regional Park for drawing our attention to the field site and for allowing and helping the deployment of a scientific experiment in a protected area. Most of the computations were performed at the 'Service Commun de Calcul Intensif de l'Observatoire de Grenoble (SCCI)'. The authors are also grateful to the 'parc national Sismob (INSU-CNRS)' and to the ISTerre for lending the seismic instruments. R. Biron transmitted the meteorological data, by courtesy of the 'Laboratoire d'étude des Transferts en Hydrologie et Environnement'. We thank the editor, Dr. Frank Krueger, as well as Dr. Valerio Poggi and one anonymous reviewer for their comments and suggestions.

## REFERENCES

Allemang, R.J. & Brown, D.L., 1982. A correlation coefficient for modal vector analysis, in *Proceedings of 1st International Modal Analysis Conference (IMAC)*, Orlando, Florida.

Bergman, T.L., Incropera, F.P., Lavine, A.S. & Dewitt, D.P., 2011. *Fundamentals of Heat and Mass Transfer*, 7th edn, Wiley, Hoboken, NJ.

Bost, M., 2009. Altération par le gel des massifs rocheux : Etude expérimentale et modélisation des mécanismes de génération des contraintes dans les fissures, *PhD thesis*, Ecole Nationale des Ponts et Chaussées, Paris, France.

Brincker, R., Zhang, L. & Andersen, P., 2001. Modal identification of output only systems using frequency domain decomposition, *Smart Mater. Struct.*, **10**, 441–445.

Burjánek, J., Gassner-Stamm, G., Poggi, V., Moore, J.R. & Fäh, D., 2010. Ambient vibration analysis of an unstable mountain slope, *Geophys. J. Int.*, **180**(2), 820–828.

Burjánek, J., Moore, J.R., Yugsi Molina, F.X. & Fäh, D., 2012. Instrumental evidence of normal mode rock slope vibration, *Geophys. J. Int.*, **188**(2), 559–569.

Clinton, J.F., Case Bradford, S., Heaton, T.H. & Favela, J., 2006. The observed wander of the natural frequencies in a structure, *Bull. seism. Soc. Am.*, **96**(1), 237–257.

Doebbling, S.W., Farrar, C.R., Prime, M.B. & Shevitz, D.W., 1996. Damage identification and health monitoring of structural and mechanical systems from changes in their vibration: a literature review. Technical Report LA-13070-MS, Los Alamos National Lab., NM (United States).

Gruber, S. & Haerberli, W., 2007. Permafrost in steep bedrock slopes and its temperature-related destabilization following climate change, *J. geophys. Res.*, **112**, F02S18, doi:10.1029/2006JF000547.

Herak, M. & Herak, D., 2009. Continuous monitoring of dynamic parameters of the DGFSM building (Zagreb, Croatia), *Bull. earthq. Eng.*, **8**, 657–669.

Jiji, L.M., 2010. *Heat Convection*, 2nd edn, Springer, Berlin, Heidelberg, New York, 543 p.

Kim, J.T. & Stubbs, N., 2003. Crack detection in beam-type structures using frequency data, *J. Sound Vibrat.*, **259**(1), 145–160.

Kukkonen, I.T. & Safanda, J., 2001. Numerical modelling of permafrost in bedrock in northern Fennoscandia during the Holocene, *Glob. Planet. Change*, **29**, 259–273.

Lévy, C., Baillet, L., Jongmans, D., Mouro, P. & Hantz, D., 2010. Dynamic response of the Chamousset rock column (Western Alps, France), *J. geophys. Res.*, **115**, F04043, doi:10.1029/2009JF001606.

Lévy, C., Jongmans, D. & Baillet, L., 2011. Analysis of seismic signals recorded on a prone-to-fall rock column (Vercors massif, French Alps), *Geophys. J. Int.*, **186**, 296–310.

Lin, Y.Q., Ren, W.X. & Fang, S.E., 2011. Structural damage detection based on stochastic subspace identification and statistical pattern recognition: II. Experimental validation under varying temperature, *Smart Mater. Struct.*, **20**, 115010, doi:10.1088/0964-1726/20/11/115010.

Lowrie, W., 2007. *Fundamental of Geophysics*, Cambridge University Press, Cambridge.

Matsuoka, N., 2001. Direct observation of frost wedging in Alpine bedrock, *Earth Surf. Process. Landforms*, **26**, 601–614.

Michel, C., Guéguen, P. & Bard, P.Y., 2008. Dynamic parameters of structures extracted from ambient vibration measurements: an aid for the seismic vulnerability assessment of existing buildings in moderate seismic hazard regions, *Soil Dyn. earthq. Eng.*, **28**, 593–604.

Michel, C., Guéguen, P., El Arem, S., Mazars, J. & Kotronis, P., 2010. Full-scale dynamic response of an RC building under weak seismic motions using earthquake recordings, ambient vibrations and modeling, *Earthq. Eng. Struct. Dyn.*, **39**(4), 419–441.

Mikael, A., Guéguen, P., Bard, P.Y., Roux, P. & Langlais, M., 2012. Long-term frequency and damping wandering in buildings analyzed using the random decrement technique, *Bull. seism. Soc. Am.*, **103**(1), doi:10.1785/0120120048.

Moore, J.R., Gisichig, V., Burjánek, J., Loew, S. & Fäh, D., 2011. Site effects in unstable rock slopes: dynamic behavior of the Randa instability (Switzerland), *Bull. seism. Soc. Am.*, **101**(6), 3110–3116.

Nayeri, R.D., Masri, S.F., Ghanem, R.G. & Nigbor, R.L., 2008. A novel approach for the structural identification and monitoring of a full-scale 17-story building based on ambient vibration measurements, *Smart Mater. Struct.*, **17**(2), doi:10.1088/0964-1726/17/2/025006.

Noetzi, J., Gruber, S., Kohl, T., Salzmann, N. & Haerberli, W., 2007. Three-dimensional distribution and evolution of permafrost temperatures in idealized high-mountain topography, *J. geophys. Res.*, **112**, F02S13, doi:10.1029/2006JF000545.

Petrovic, J.J., 2003. Review mechanical properties of ice and snow, *J. Mater. Sci.*, **38**(1), 1–6.

Sohn, H., Dzwonczyk, M., Straser, E.G., Kiremidjian, A.S., Law, K.H. & Meng, T., 1999. An experimental study of temperature effect on modal parameters of the Alamosa canyon bridge, *Earthquake Eng. Struct. Dyn.*, **28**, 879–897.

Stubbs, I.R. & McLamore, V.R., 1973. The ambient vibration survey, in *Proceedings of Fifth World Conference on Earthquake Engineering*, Rome, Italy, pp. 286–289.

Tourenq, C., 1970. La gélivité des roches: application aux granulats. Research Report n°6, Laboratoire Central des Ponts et Chaussées, Paris, 60 p.

Wegmann, M., Gudmundsson, G.H. & Haeberli, W., 1998. Permafrost changes in rock walls and the retreat of Alpine glaciers: a thermal modelling approach, *Permafrost Periglacial Process.*, **9**, 23–33.

Xia, Y., Xu, Y.L., Wei, Z.L., Zhu, H.P. & Zhou, X.Q., 2010. Variation of structural vibration characteristics versus non-uniform temperature distribution, *Eng. Struct.*, **33**(1), 146–153.

Yuean, K.V. & Kuok, S.C., 2010. Modeling of environmental influence in structural health assessment for reinforced concrete buildings, *Earthq. Eng. Eng. Vib.*, **9**, 295–306.